

# 5

---

## *Growth of Sn-alloyed group IV materials for photonic and electronic applications*

---

Henry H. Radamson<sup>a</sup> and Mahdi Moeen<sup>a, b</sup>

<sup>a</sup>Department of Devices and Circuits, KTH Royal Institute of Technology, Isafjordsgatan 22-26, 16640 Kista, Sweden

<sup>b</sup>Nocilis Materials, Isafjordsgatan 39, 16440 Kista, Sweden

### Outline:

Introduction.....	130
GeSn(Si) as channel material in MOSFETs.....	130
GeSn(Si) alloys for photonic applications.....	131
Methods of characterizing the composition and strain in GeSn(Si) materials.....	133
Sn incorporation.....	135
GeSn Nano-Dots.....	139
Incorporation of dopants in GeSn alloys.....	141
Multilayer structures of GeSn/Ge for IR detection or emission.....	142
Conclusions.....	142
References.....	143

## Introduction

Different Ge-Sn-Si alloys have been known for over twenty years for their excellent electronic and photonic properties [1], [2]. Earlier, these alloys were deposited by molecular beam epitaxy (MBE) [3], however, the growth of these alloys using CVD technique was not demonstrated until recently when stable Sn precursors were produced [4], [5].

Pressure chemical vapor deposition (CVD) is a process widely used in the semiconductor industry to grow Si-based materials. Various precursors for Si deposition depending on the growth temperature and application are used: silane ( $\text{SiH}_4$ ), disilane ( $\text{Si}_2\text{H}_6$ ), trisilane ( $\text{Si}_3\text{H}_8$ ) and dichlorosilane ( $\text{SiH}_2\text{Cl}_2$ ). Common sources for Ge deposition are germane ( $\text{GeH}_4$ ) and digermane ( $\text{Ge}_2\text{H}_6$ ). There are also a variety of  $(\text{H}_3\text{Ge})_x\text{SiH}_{4-x}$  ( $x=1-4$ ) compounds for the growth of Ge-rich SiGe layers [4]. The dopant precursors used are diborane ( $\text{B}_2\text{H}_6$ ) for p-type doping and phosphine ( $\text{PH}_3$ ) and arsine ( $\text{AsH}_3$ ) for n-type doping.  $\text{As}(\text{GeH}_3)_3$  is a gas source which is also used for n-type doping of SiGe layers at low growth temperature [4]. These sources are usually diluted in hydrogen. Methylsilane ( $\text{SiH}_3\text{CH}_3$ ) is widely used for carbon doping in Si and SiGe layers. For Sn,  $\text{SnD}_4$  and  $\text{SnCl}_4$  are the most practical and common sources. Although  $\text{SnD}_4$  has demonstrated impressive results, the  $\text{SnD}_4$  molecule has a limited lifetime and dissociates into Sn and deuterium. The stability problem can be partly solved and prolonged to a few months when  $\text{SnD}_4$  is diluted in hydrogen. However, producing a commercial  $\text{SnD}_4$  source is still an obstacle for CVD growth.

Another source for Sn is  $\text{SnCl}_4$  which is broadly used to grow Sn oxides for atomic layer deposition (ALD). This source is in liquid phase and transformed into gas phase which is then introduced into the CVD reactor. High quality GeSn layers with high Sn content have been deposited in temperature range of 290-380 °C [6, 7]. Figure 5.1 shows how to grow GeSn layers with different strain types.

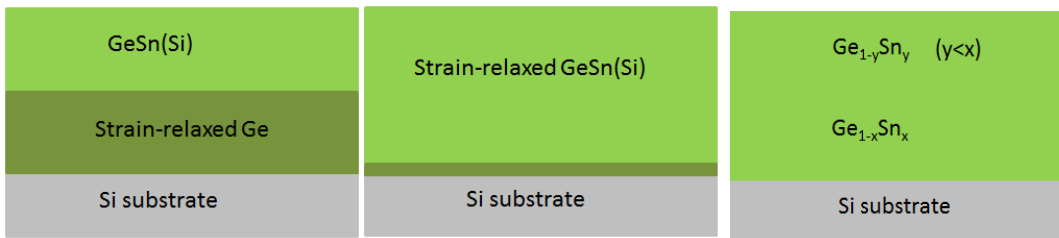


**FIGURE 5.1**  
Schematic showing growth of strained GeSn with different types of strain

## GeSn(Si) as channel material in MOSFETs

The channel mobility is an important characteristic of MOSFETs.

Figure 5.2 shows three ways to integrate GeSn(Si) layers in high performance MOSFETs. In Figure 5.2(a) the channel layer has a compressive strain and the Ge buffer is strain free. As a result of the valence band offset, such design is intended to improve the hole mobility. For pMOSFETs with  $\text{Ge}_{0.93}\text{Sn}_{0.07}$ , an improvement of 85% in hole mobility compared to Ge has been reported [2].

Inducing compressive strain in MOSFETs can be realised either in two dimensions as in Figure 5.2(a) or in one dimension when Ge channel is stressed by GeSn grown in source/drain (S/D) areas as shown in Figure 5.2(b).

In this case, the channel is uniaxially strained compared to the previous case which was biaxially strained. The benefits of uniaxially strained channels are discussed in numerous reports and addressed as: higher drift current, high hole mobility in response to both high and low applied electric fields and smaller shift of threshold voltage compared to biaxial strain.

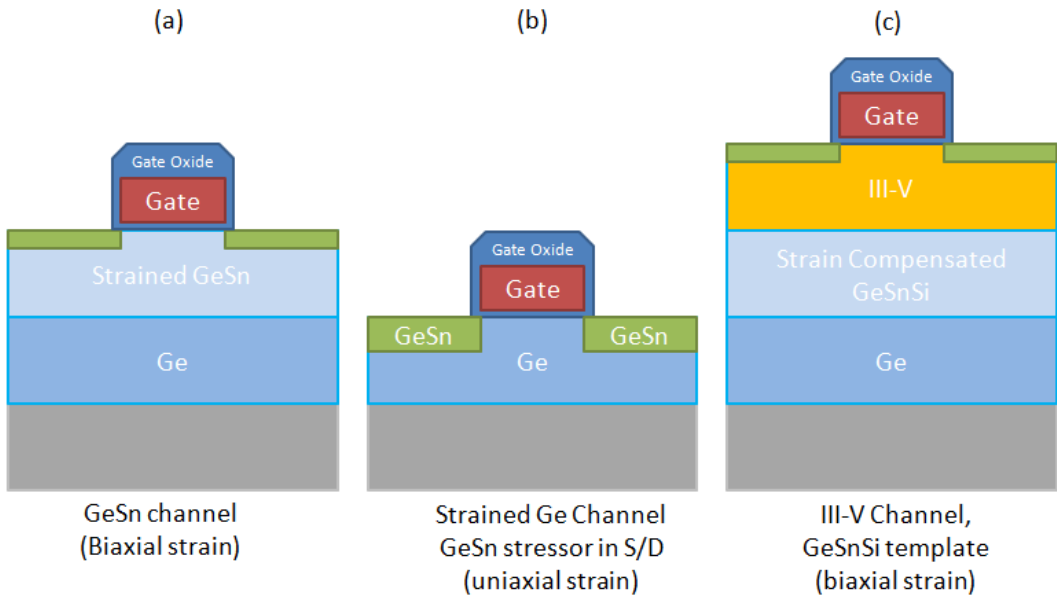


**FIGURE 5.2**

Three possible ways to integrate GeSn(Si) layers in high performance MOSFETs

To further improve the carrier mobility group IV channel materials may be replaced with more conductive semiconductors. Recent reports propose III-V materials (GaAs, InP, InAs and InSb) as channel materials [8]. The low electron mass of III-V semiconductors due to their small bandgap can be applied in high electron mobility transistors (HEMTs) [8]. For example, mobility enhancement to the value of  $27300 \text{ cm}^2/\text{Vs}$  has been reported for epitaxially grown AlGaSb/InAs on Si substrate [9]. The large lattice mismatch between III-V materials and Si however makes the growth a challenging task. It has been suggested that GeSnSi intermediate layers will solve this problem. The lattice constant of GeSnSi can be modified by changing the Si and Sn content in Ge and makes a lattice-matched layer to a certain III-V material thus most of defects will be located in GeSnSi layer and high quality III-V compounds may be grown [10].

## GeSn(Si) alloys for photonic applications

Obtaining light emission from Si-based materials is a challenge due to the indirect band gap of this material. Silicon has a conduction band minimum at the X point (bandgap of 1.12 eV) while for Ge it

is located at the L point. Both Si and Ge have another conduction band minimum at the  $\Gamma$ -point (so-called photonic bandgap) estimated to be 3.2 and 0.8 eV for Si and Ge, respectively. Since the energy difference between the L and  $\Gamma$  valleys ( $\Delta E_{\Gamma L}$ ) for Ge is 140 meV, it is highly likely that Ge shows a direct transition. Any such transition is however still a mixture of both direct and indirect transitions. The wavelength of direct transition in Ge material is  $\sim 1.55 \mu\text{m}$  which is located in telecom wavelength region.

Inducing tensile strain in Ge matrix and/or highly n-type doping improve the luminescence emission efficiency. A pure direct transition may occur when  $\Delta E_{\Gamma L}$  of Ge becomes as small as possible. By applying strain engineering, the bandgap can be modified by alloying Ge with Sn, Si or C atoms. For Ge, the bandgap narrowing occurs for both L and  $\Gamma$  bands simultaneously as a response to alloying. Meanwhile, the narrowing of  $\Gamma$ -band is larger than L-band ( $\Delta E_{\Gamma L}$  decreases). In case of GeSn/Ge heterostructure,  $\Delta E_{\Gamma L}$  can approach zero for a Sn content around 6-8% as shown in

FIGURE 5.3.

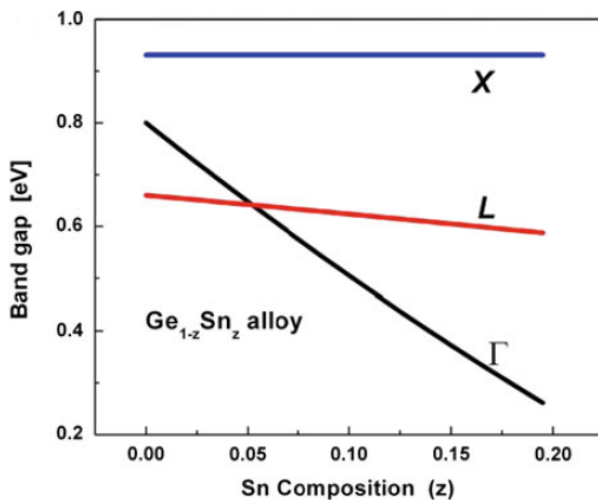


**FIGURE 5.3**

Bandgap energy of direct and indirect gaps of GeSn versus Sn content. Indirect-to-direct transition may occur when L and  $\Gamma$  lines meet [11]

The major benefit of Sn-alloys is the ability to achieve an indirect-to-direct bandgap transition when 6-8% Sn is implemented in the GeSn matrix. These GeSn layers have narrower bandgap than Ge which may lead to emission or detection in the IR region. Optically pumped Ge-on-Si lasers for wavelength of  $1.6 \mu\text{m}$  are already shown [12]. Recent simulations propose the Ge-Sn-Si materials as suitable alloys for electrically pumped lasers as light sources, in the following structures:

- I. Lattice matched Ge/Ge<sub>1-x-y</sub>Si<sub>x</sub>Sn<sub>y</sub> structures for intersubband transitions (IST) in quantum cascade lasers (QCL). Intersubband transitions occur at the L-valley.
- II. Lattice matched GeSn/GeSiSn structures in form of a multiple quantum well (MQW). This structure functions on band-to-band (or interband) transitions occurring at  $\Gamma$ -valley (type I).

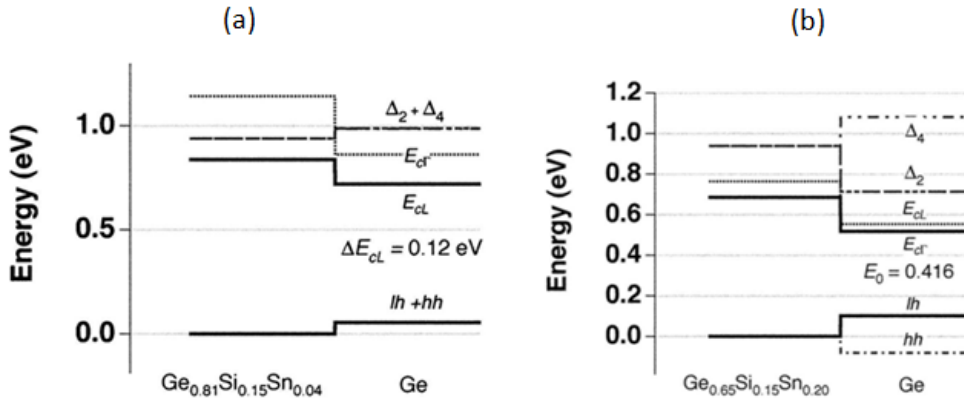


**FIGURE 5.4**  
Illustration of laser design a) IST at L-valley [13] and b) interband transition at  $\Gamma$ -valley [14]

Ternary  $\text{Ge}_{1-x-y}\text{Sn}_y\text{Si}_x$  alloys offer the possibility to modify the band structure independently from strain by adjusting the Si and Sn contents in the alloys. The calculated energy bandgap of GeSnSi materials shows that a lattice matched  $\text{Ge}/\text{Ge}_{0.76}\text{Si}_{0.19}\text{Sn}_{0.05}$  structure is an appropriate choice for QCL [11].

## Methods of characterizing the composition and strain in GeSn(Si) materials

As discussed previously, tailoring the strain in the epitaxial layers is important because it impacts the mechanical, electrical and optical properties of layers. In group IV materials, Sn has the biggest atomic radius whereas C is considered as the smallest atom which can be integrated to induce strain in Si or Ge lattices. The strain profile (type and amount) in epi-layers is designed by the appropriate choice of the buffer layer (or virtual substrate), composition of the alloy and atomic size difference (to Si or Ge). For example,  $\text{Ge}_{1-x}\text{Sn}_x$  layers can be grown strained or relaxed on Si or Ge according to the structures shown in Figure 5.1.

In these cases, the bandgap is engineered by the strain amount or/and alloying with Sn. The Sn content in GeSn layers can be measured by using Rutherford backscattering spectrometry (RBS), Raman spectroscopy and X-ray diffractometry (XRD) techniques. For the XRD technique, the substitutional Sn content is extracted from lattice parameters.

XRD maps of three GeSn layers deposited at different growth temperatures are shown in FIGURE 5.5. Using the high resolution reciprocal lattice maps (HRRLMs), it is possible to study the effect of growth temperature on Sn content and the layer quality of GeSn layers. As expected from the large lattice mismatch between GeSn and Si, the maps demonstrate a broadening in  $\omega$ -direction that is an indicator of defects in the grown crystal. All the three samples therefore appear to have similar defect density. However, more precise and easier analysis is only possible by TEM and SEM tools.

In this example, the grown GeSn layers are relaxed and extracting their Sn content is possible by calculation of the lattice mismatch parameters. In strained layers, the Sn content is easier to find out just by using rocking curves and extraction of strain in the grown layer. To find out the mismatch parameters, parallel and perpendicular to the growth direction, the GeSn and Si peaks in the reciprocal space (maps) are used, giving values for  $\theta_s$  and  $\omega_s$  for Si substrate and  $\theta_l$  and  $\omega_l$  for the GeSn layer. These values are used in the following key equations [15], [16]:

$$f_{\perp} = \frac{\sin \theta_s \cos(\omega_s - \theta_s)}{\sin \theta_l \cos(\omega_l - \theta_l)} - 1 \quad (1)$$

$$f_{\parallel} = \frac{\sin \theta_s \sin(\omega_s - \theta_s)}{\sin \theta_l \sin(\omega_l - \theta_l)} - 1 \quad (2)$$

The lattice mismatch is then given by:

$$f = (f_{\perp} - f_{\parallel}) \frac{1-\nu}{1+\nu} + f_{\parallel} \quad (3)$$

in which  $\nu$  is the Poisson ratio for  $\text{Ge}_{1-x}\text{Sn}_x$  and represents the initial establishment of mismatch of the cubic crystal from mismatch parameters. It is expressed by elastic parameters,  $C_{12}$  and  $C_{11}$  [17], as follows [18]:

$$\nu = C_{12} / (C_{11} + C_{12}) \quad (4)$$

Using Vegard's rule, the  $C_{ij}$  values for an alloy is found by:

$$C_{ij}(\text{GeSn}) = (1-x) C_{ij}(\text{Ge}) + x C_{ij}(\text{Sn}) \quad (5)$$

Once the lattice mismatch is found, the GeSn lattice constant can be found by:

$$a_{\text{GeSn}} = (f+1) \cdot a_{\text{Si}} \quad (6)$$

Then, again by applying the Vegard's rule for lattice constant of GeSn alloy and solving the resulting equation for  $x$ , Sn content ( $x$ ) is found [19]:

$$a_{\text{GeSn}}(x) = a_{\text{Sn}} x + \theta_{\text{SnGe}} x(1-x) + a_{\text{Ge}}(1-x) \quad (7)$$

where  $\theta_{\text{SnGe}}$  is a constant which relates to GeSn alloying and is  $0.166 \text{ \AA}$  for  $x \leq 0.20$  [19]. As an example, the Sn content in three strain-relaxed GeSn layers grown at different temperatures have been estimated by HRRLMS (FIGURE 5.5) and RBS spectra and are shown in TABLE 5.1. Calculated Sn contents by these techniques for different temperatures are shown to be in good agreement [20].

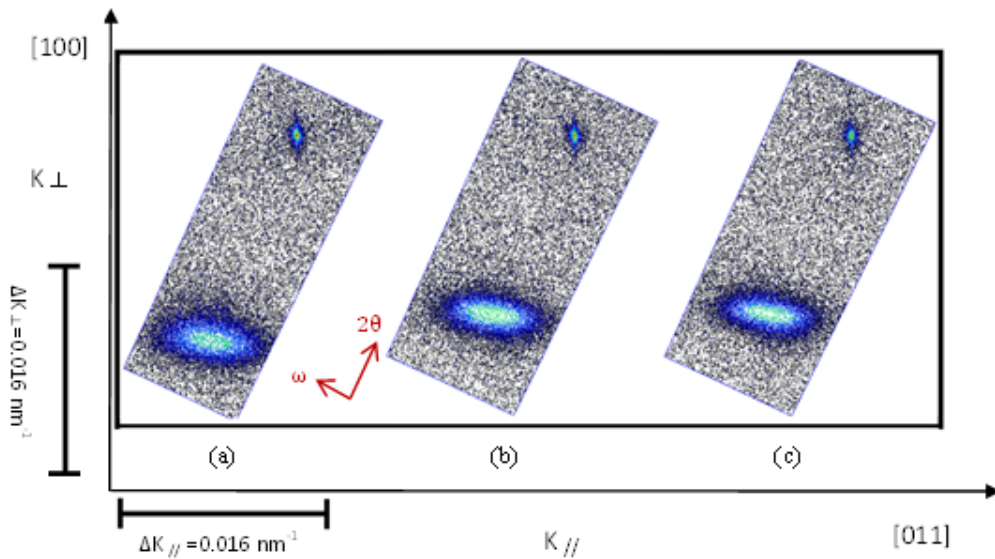


**FIGURE 5.5** High resolution reciprocal lattice maps (HRRLMs) in (113) reflection of three strain-relaxed GeSn layers deposited at growth temperatures of (a) 290 °C, (b) 350 °C and (c) 380 °C (where  $\omega$ : incident angle and  $2\theta$ : reflected angle) [20]

**TABLE 5.1** Sn content in GeSn layers obtained by HRRLMs (FIGURE 5.5) and RBS [20]

GeSn growth temp.	HRRLMs (%)	RBS (%)
290 °C	2.61	2.7
350 °C	1.55	1.5
380 °C	1	0.92

## Sn incorporation

Sn incorporation is one of the main issues in the process of GeSn layer growth. At low growth temperatures, GeSn layers with Sn contents up to 6% can be grown with high Sn incorporation. FIGURE 5.6 shows a multi quantum well structure in which GeSn wells of various compositions are sandwiched between Ge barrier layers. GeSn layers sustain compressive strain as they are grown on much thicker Ge layers.

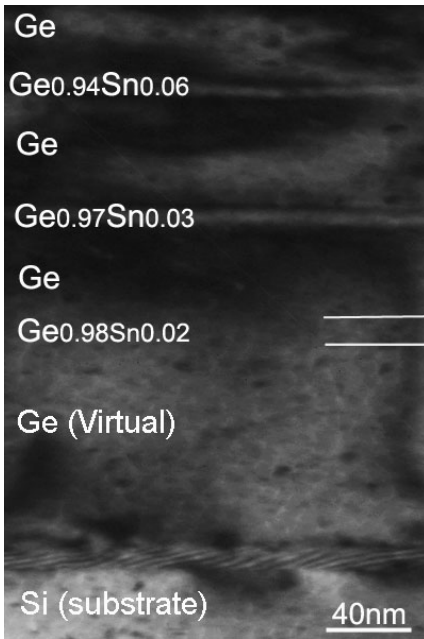


**FIGURE 5.6**  
 TEM image of a multi quantum well structure (MQW) of Ge<sub>1-x</sub>Sn<sub>x</sub>/Ge [7]

SEM micrographs in Figure 5.7 show the surface of relaxed GeSn layers grown at different temperatures (290, 350 and 380 °C). By increasing the growth temperature, the surface roughness gets worse. This is partly due to the formation of dots in the beginning of GeSn growth step, which can be minimized by optimizing the Sn flow. However, the more critical reason for the surface roughness is Sn surface segregation which is more evident at higher temperatures, leading to a mixture of lateral and 3D growth. Sn segregation is itself caused by the large atomic size of Sn comparing to Ge in the GeSn lattice. No matter if the GeSn layer is grown on Si or Ge substrate, the difference in atomic sizes gives rise to a large elastic energy in the GeSn crystal pushing up the Sn atoms towards the surface.

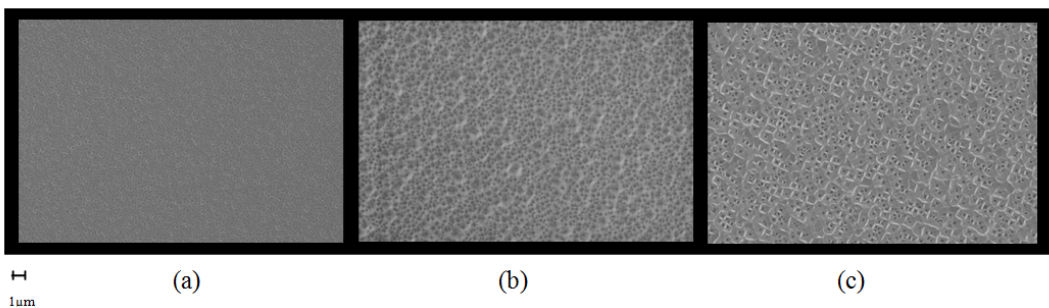
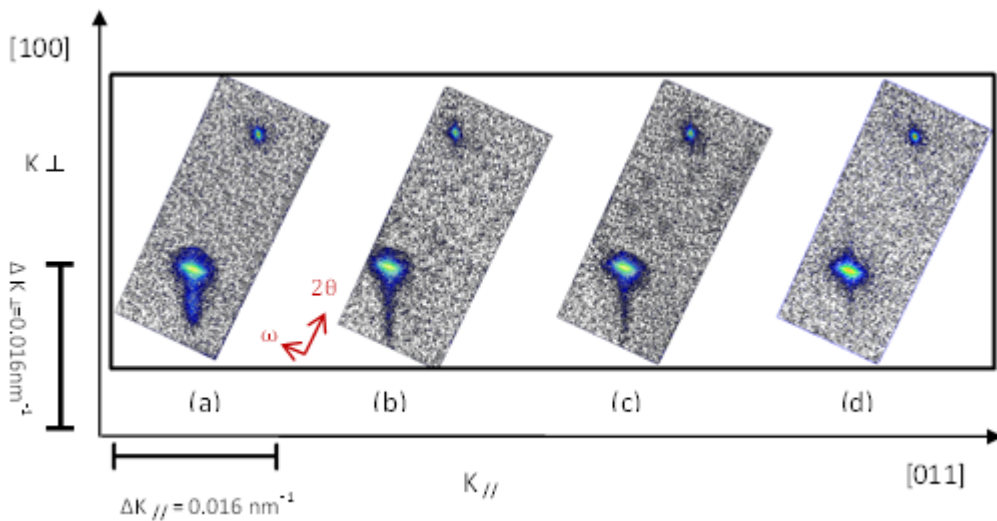


**FIGURE 5.7**  
 SEM micrographs showing the surface morphology of relaxed GeSn layers grown at (a) 290 °C (b) 350 °C and (c) 380 °C [20]



A possible way to handle the size difference effect is to control the excess of crystal energy, which will be thermodynamically favorable and will result in lower Sn segregation. For instance, in the GeSnSi ternary crystal, the strain amount is more balanced, comparatively, due to the small size of Si, which compensates the large atomic size of Sn. The same result can be achieved by introducing any atoms smaller than Ge, for example boron, phosphorous and carbon [7].

Using methylsilane ( $\text{SiCH}_3$ ) as a gas source for incorporating both carbon and silicon, a series of GeSnSi(C) samples were grown on Ge at 290 °C with different  $\text{Si}_2\text{H}_6$  and  $\text{SiCH}_3$  partial pressures. A smooth relaxed buffer layer of Ge was grown in two steps at 400 and 650 °C on top of which the 10 nm thick strained GeSnSi(C) layers were deposited. The top layers were intentionally grown as thin as 10 nm to avoid strain relaxation. HRRLMs of these samples are shown in Figure 5.8 For XRD mapping, the (113) reflection was chosen to provide high enough sensitivity for characterization of such thin layers.

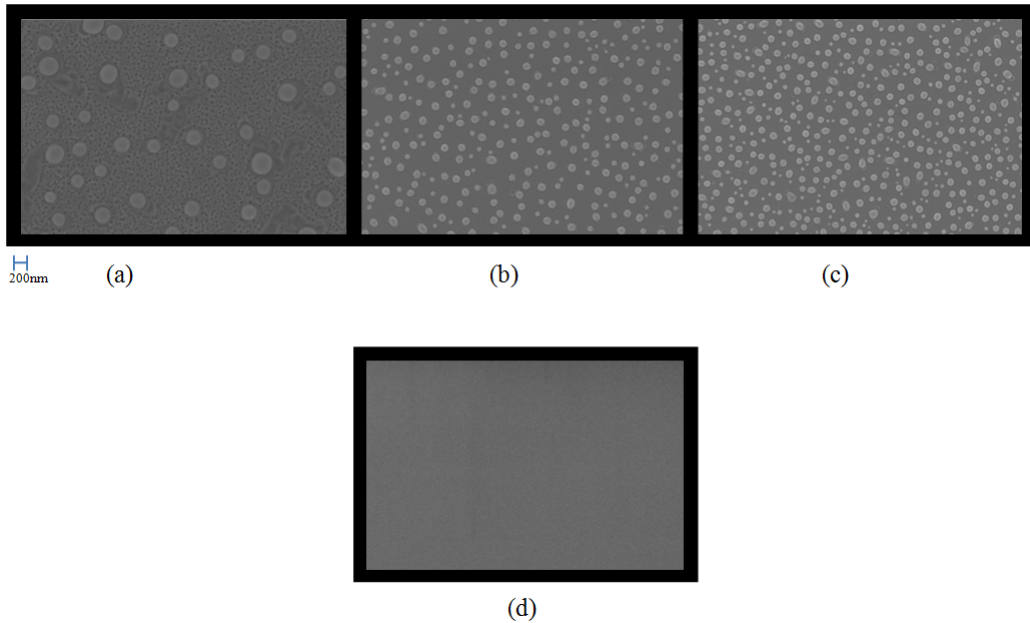


**FIGURE 5.8**

HRRLMs of three GeSn(Si) samples grown by  $\text{Si}_2\text{H}_6$  with partial pressure of (a) 0, (b) 10 and (c) 40 mtorr, and a GeSnSiC sample grown by  $\text{SiCH}_3$  partial pressure of 2.5 mtorr [20]

XRD maps of the three first samples (Figure 5.8(a-c)) show compressive strain in the GeSn layers as the GeSn peak is aligned with the Ge peak in  $K_{//}$ -direction. It is also observed that by increasing Si partial pressure the amount of the compressive strain, which is indicated by the distance between Ge and GeSn peaks, decreases. In the fourth sample (Figure 5.8(d)) containing C in addition to Si, the strain is totally compensated (GeSn and Ge peaks overlay). The Sn-content in Figure 5.8(a) is measured to 3% while the strain is partially compensated with 12% Si in Figure 5.8(c).

Figure 5.9 shows HRSEM micrographs of the above samples to analyse their surface morphology.

**FIGURE 5.9**

Surface HRSEMs of GeSnSi(C) layers grown on a Ge buffer layer with various Si and C source partial pressures corresponding to FIGURE 5.8 [20]

As shown previously for relaxed GeSn layers, Sn segregates are visible on the layer surfaces. In the absence of Si, the largest segregates show up (Figure 5.9(a)). By increasing the amount of Si, segregates get smaller in size (Figure 5.9(b)) and less dense (Figure 5.9(c)) until they eventually almost disappear by introduction of carbon (Figure 5.9(d)). The increase of Sn incorporation in GeSnSi layers is due to strain compensation by Si atoms in Ge matrix and reduction of the crystal energy.

To further investigate the effect of strain on Sn incorporation, a sample with graded Si content in GeSn has been grown and measured by RBS as shown in Figure 5.10. The Si partial pressure has been increased in three steps 20, 40 and 80 mtorr.

Figure 5.10(a) shows GeSn layers without Si. The Sn content is calculated to be 3.6%. However, with similar growth conditions the GeSnSi layer contains 30% Sn as shown in Figure 5.10(b).

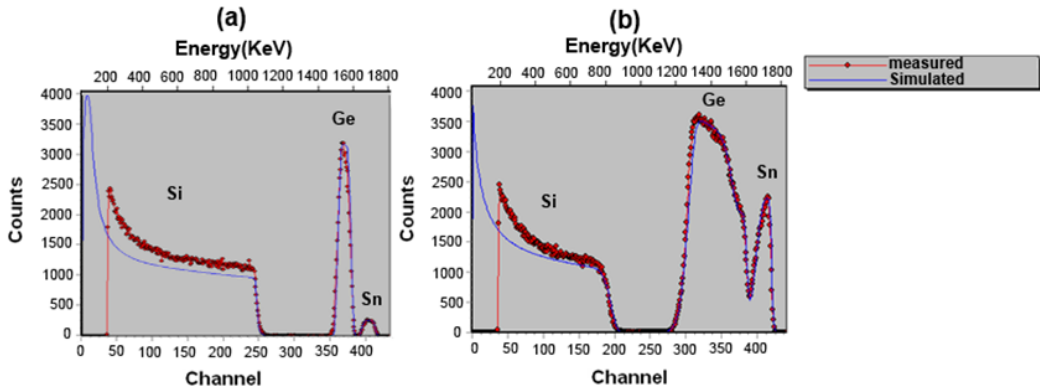


**FIGURE 5.10**

RBS spectra for (a)  $\text{Ge}_{0.965}\text{Sn}_{0.035}$  and (b) GeSnSi layer with a graded Si flux but constant Sn flux during epitaxy

In addition to improving the surface quality, GeSnSi(C) layers can be used in photonic applications due to their tunable bandgap which is predicted to be between 0.86-1.4 eV depending on the composition [5]. Incorporation of Si and C atoms in GeSn layers, however, is not always straightforward. For instance, relaxed GeSn layers are reported as not adopting Si and C in their crystal structure as easily as strained layers [20].

## GeSn Nano-Dots

Formation of nano-dots of GeSn is another potential for photonic applications. Quantum confinement effect has been reported for GeSn quantum dots. By the quantum confinement effect it is possible to tailor the bandgap by changing the size of the quantum dot. As the GeSn material is expected to have direct bandgap transition for high amounts of Sn, GeSn dots can be advantageous by the higher bandgap they can offer (compared to high Sn content GeSn films) [21].

For CVD growth, so far, formation of nano-dots with increased Sn content is reported. Variation of Sn content can be used for changing the bandgap and hence the operating wavelength of detectors or light emitters. A possible way of growing nano-dots of GeSn is by thermal treatment of CVD grown GeSn layers. At higher temperatures (>500 C) Sn surface atoms start to segregate and form nano-dots. Robert Chen et al. [22] reported on the process of formation of the dots and their sizes by the applied thermal budget (TABLE 5.2).

**TABLE 5.2**

Summary of the annealing treatments along with the sample RMS surface roughness determined using atomic force microscopy. Samples annealed at 450 °C and above show signs of nanodot formation as seen by a variety of material analysis techniques [22]

Sample	Recipe	RMS surface roughness for flat regions (area in $\mu\text{m}^2$ )	Surface features (d=diameter, h=height)
AG	None, as-grown	0.21 nm (5x5)	Smooth
AG-Etch	GeSn film etched	0.61nm (5x5)	Slightly-increased roughness
400°C-60	400 °C, 60 s Anneal	0.21 nm (5x5)	Smooth
400°C-180	400 °C, 180 s Anneal	0.17 nm (5x5)	Smooth
400°C-500	450 °C, 500 s Anneal	0.19 nm (5x5)	Smooth
450°C-60	450 °C, 60 s Anneal	0.19 nm (2.5 x 0.8 flat)	Nanodot formation (d=410 nm, h=110 nm), 0.08 dots/ $\mu\text{m}^2$ )
500°C-60	500 °C, 60 s Anneal	0.17 nm (3x1 flat)	Nanodot formation (d=390 nm, h=100 nm), 0.09 dots/ $\mu\text{m}^2$ )
500°C-60 HCl	500 °C, 60 s Anneal with an 8 s HCl Etch	0.23 nm (4x1 flat)	Similar to 500°C-60s with 40 nm-deep voids instead of dots

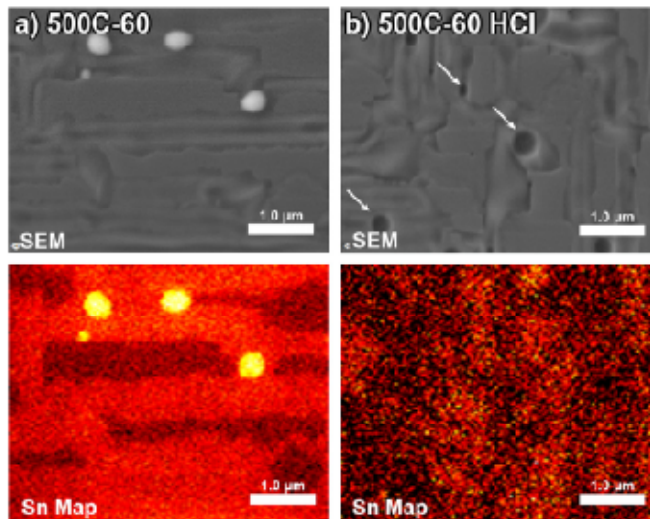


**FIGURE 5.11**

Scanning electron micrographs (top) and Auger surface maps (bottom) of Sn for sample 500°C-60 in TABLE 5.2 (a) before and (b) after etching with HCl [22]

They have also reported on the higher Sn content of the dots by Auger electron spectroscopy. This, however, shows only that the dots' surface is Sn rich. Appearance of voids in place of dots after

etching by HCl (FIGURE 5.11) may be a sign of the difference in their composition or phase comparing to the GeSn film upon which they are placed. Another way to make GeSn nano-dots without excessive thermal treatment is the growth of GeSn layers at higher temperature (e.g. 380 °C) where the Sn may segregate to the surface. The segregated Sn forms Sn islands whose size depends on Sn partial pressure, growth temperature and deposition time.

### Incorporation of dopants in GeSn alloys

Doped semiconductors, used mainly as contact layers to lower the resistivity, are essential in electronic and photonic devices. Thus, doping of GeSnSi(C) layers (both n-type and p-type) is of great interest. Typical gas sources for n-type and p-type doping are diborane (B<sub>2</sub>H<sub>6</sub>) and phosphine (PH<sub>3</sub>), respectively, and a typical doping level for a p-i-n diode structure, used in photonic applications, is in range of  $1 \times 10^{17}$ - $1 \times 10^{19}$  cm<sup>-3</sup>. With SnD<sub>4</sub> as Sn source, growth of n-type and p-type layers at 350 °C are reported [23]. Boron doping [6], [7] and phosphorous doping [7] of GeSn layers grown by SnCl<sub>4</sub> are also carried out. Resistivity results obtained for such layers, and their substitutional Sn content are shown in Figure 5.12. For phosphorous doping, the higher resistivity in 290 °C can be explained by lower solid solubility of phosphorous in germanium compared to 310 °C whilst the resistivity of boron doped layers is less sensitive to growth temperature. This shows that boron incorporation reaches a saturation level and does not change much with increasing temperature. The slight increase in the Sn content of the layers in higher dopant gas partial pressures can be explained by strain compensation upon introduction of smaller atoms (P and B) in the Ge lattice, as discussed previously.

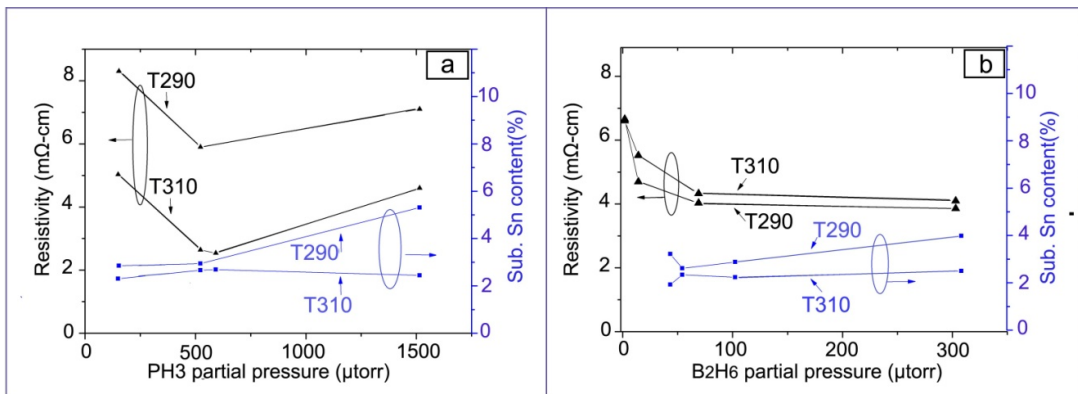


**FIGURE 5.12** Resistivity results and substitutional Sn content of (a) phosphorous and (b) boron doped GeSn layers vs dopant source gas partial pressure [7]

More accurate insight about the layer composition and conductivity can be achieved by SIMS and Hall measurements. SIMS measurements on the above samples at the highest dopant partial pressures at 310 °C suggest  $1 \times 10^{20}$  and  $5 \times 10^{18}$  cm<sup>-3</sup> P and B doping concentrations, respectively, which satisfies the device requirements.

### Multilayer structures of GeSn/Ge for IR detection or emission

A complete detector or laser structure demands sharp interfaces with abrupt dopant profile. A structure containing GeSn/Ge superlattice in from of type I or II alignment can serve for detection or emission of light in infrared region.

FIGURE 5.13(a) and (b) show (113) HRRLMs of a GeSn/Ge multilayer with a p-i-n profile where the initial Ge layer (at the bottom side) is strain-free and the Ge cap layer is tensile strained. There is a slight shift of GeSn peak from Ge peak along  $k_{\perp}$  direction which is a sign of partial strain relaxation in the GeSn (or GeSnSi) layers. The top B-doped Ge cap layer is therefore expected to have tensile strain. If the doping level of the cap layer is chosen high enough, it is possible to fill the L valley of the Ge conduction band to facilitate the direct  $\Gamma$  gap transitions. By changing the amount of Si content it is then possible to manipulate the bandgap (reported between 0.8 to 1.2 eV [7]), thus operating wavelength of the device. It is reported that total strain compensation in these devices are achieved with a Si content of 12%.

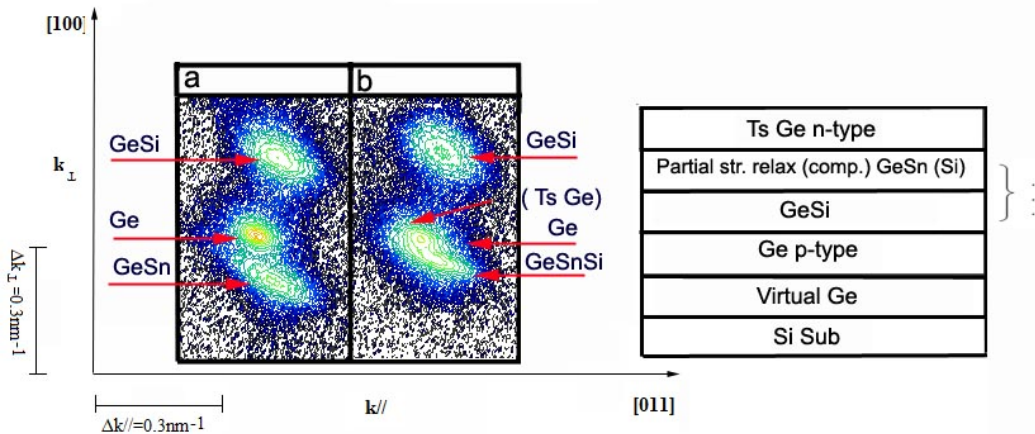


**FIGURE 5.13** HRRLMs of p-i-n structures containing (a) GeSi/GeSn and (b) GeSi/GeSnSi in their intrinsic part (three GeSn quantum wells sandwiched between GeSi barriers). The Ge cap layer is expected to have tensile strain (denoted by Ts)

### Conclusions

$Ge_{1-x}Sn_x$  layers ( $0.01 \leq x \leq 0.30$ ) have been successfully grown using  $SnCl_4$  as Sn source at low temperature range of 290°C to 380°C by LPCVD. The GeSn dots can also be formed by annealing GeSn layers or applying growth temperatures as high as 380 °C. High-resolution reciprocal lattice mapping is an accurate method to measure the Sn content in GeSn which is consistent with Rutherford backscattering technique.

Phosphorus and boron doped GeSn layers with atomic concentrations of ( $10^{17}$ - $10^{20} \text{ cm}^{-3}$  and  $10^{17}$ - $5 \times 10^{18} \text{ cm}^{-3}$ ) respectively, were grown using  $PH_3$  and  $B_2H_6$  gas sources. The GeSnSi layers were grown using  $Si_2H_6$  as Si precursor and the strain was tailored by Si or Sn content. The Sn content in

B- and P-doped GeSn was enhanced by increasing of dopant concentration showing that a balance between a compressive and tensile strain is favorable for incorporating more Sn in the Ge matrix.

These results show that GeSnSi(C) alloys with varying Sn and Si contents can be grown using RPCVD. These layers are the key elements for a monolithic solution for Si-based photonics and electronics in the near future.

## References

1. P. Moontragoon, Z. Ikonić, and P. Harrison, "Band structure calculations of Si-Ge-Sn alloys: achieving direct band gap materials," *Semicond. Sci. Technol.*, vol. 22, no. 7, pp. 742–748, Jul. 2007.
2. S. Gupta, Y.-C. Huang, Y. Kim, E. Sanchez, and K. C. Saraswat, "Hole Mobility Enhancement in Compressively Strained Ge<sub>0.93</sub>Sn<sub>0.07</sub> pMOSFETs," *IEEE Electron Device Lett.*, vol. 34, no. 7, pp. 831–833, Jul. 2013.
3. O. Gurdal, P. Desjardins, J. R. A. Carlsson, N. Taylor, H. H. Radamson, J.-E. Sundgren, and J. E. Greene, "Low-temperature growth and critical epitaxial thicknesses of fully strained metastable Ge<sub>1-x</sub>Sn<sub>x</sub> (x≤0.26) alloys on Ge(001)2×1," *J. Appl. Phys.*, vol. 83, no. 1, p. 162, 1998.
4. J. Kouvetakis, J. Menendez, and J. Tolle, "Advanced Si-based Semiconductors for Energy and Photonic Applications," *Solid State Phenom.*, vol. 156–158, pp. 77–84, Oct. 2009.
5. J. Kouvetakis, J. Mathews, R. Roucka, A. V. G. Chizmeshya, J. Tolle, and J. Menendez, "Practical Materials Chemistry Approaches for Tuning Optical and Structural Properties of Group IV Semiconductors and Prototype Photonic Devices," *IEEE Photonics J.*, vol. 2, no. 6, pp. 924–941, Dec. 2010.
6. B. Vincent, F. Gencarelli, H. Bender, C. Merckling, B. Douhard, D. H. Petersen, O. Hansen, H. H. Henrichsen, J. Meersschant, W. Vandervorst, M. Heyns, R. Loo, and M. Caymax, "Undoped and in-situ B doped GeSn epitaxial growth on Ge by atmospheric pressure-chemical vapor deposition," *Appl. Phys. Lett.*, vol. 99, no. 15, p. 152103, 2011.
7. H. Radamson, M. Noroozi, A. Jamshidi, and M. Östling, "Strain Engineering in GeSnSi Materials," *ECS Trans.*, vol. 50(9), pp. 527–531, 2013.
8. R. Chau, "Benchmarking nanotechnology for high-performance and low power logic transistor applications," in *4th IEEE Conference on Nanotechnology, 2004.*, 2004, pp. 3–6.
9. Y. C. Lin, H. Yamaguchi, E. Y. Chang, Y. C. Hsieh, M. Ueki, Y. Hirayama, and C. Y. Chang, "Growth of very-high-mobility AlGaSb/InAs high-electron-mobility transistor structure on si substrate for high speed electronic applications," *Appl. Phys. Lett.*, vol. 90, no. 2, p. 023509, Jan. 2007.
10. J. Kouvetakis, J. Tolle, R. Roucka, V. R. D'Costa, Y. Fang, A. V. Chizmeshya, and J. Menendez, "Nanosynthesis of Si-Ge-Sn Semiconductors and Devices via Purpose-built Hydride Compounds," in *ECS Transactions*, 2008, vol. 16, pp. 807–821.
11. G. Sun, "Towards Si-based electrically injected group-IV lasers," *Opt. Quantum Electron.*, vol. 44, no. 12–13, pp. 563–573, Apr. 2012.
12. J. Liu, X. Sun, R. Camacho-Aguilera, L. C. Kimerling, and J. Michel, "Ge-on-Si laser operating at room temperature.," *Opt. Lett.*, vol. 35, no. 5, pp. 679–81, Mar. 2010.

13. G. Sun, H. H. Cheng, J. Menéndez, J. B. Khurgin, and R. A. Soref, "Strain-free Ge/GeSiSn quantum cascade lasers based on L-valley intersubband transitions," *Appl. Phys. Lett.*, vol. 90, no. 25, p. 251105, Jun. 2007.
14. S.-W. Chang and S. L. Chuang, "Theory of Optical Gain of  $\text{Si}_x\text{Ge}_y\text{Sn}_{1-x-y}$  Quantum-Well Lasers," *IEEE J. Quantum Electron.*, vol. 43, no. 3, pp. 249–256, Mar. 2007.
15. H. H. Radamson and J. Hållstedt, "Application of high-resolution x-ray diffraction for detecting defects in SiGe(C) materials," *J. Phys. Condens. Matter*, vol. 17, no. 22, pp. S2315–S2322, Jun. 2005.
16. P. F. Fewster and N. L. Andrew, "Determining the lattice relaxation in semiconductor layer systems by x-ray diffraction," *J. Appl. Phys.*, vol. 74, no. 5, p. 3121, 1993.
17. S. Krishnamurthy, A. Sher, and A.-B. Chen, "Generalized Brooks' formula and the electron mobility in  $\text{Si}_x\text{Ge}_{1-x}$  alloys," *Appl. Phys. Lett.*, vol. 47, no. 2, p. 160, 1985.
18. J. J. Wortman and R. A. Evans, "Young's Modulus, Shear Modulus, and Poisson's Ratio in Silicon and Germanium," *J. Appl. Phys.*, vol. 36, no. 1, p. 153, 1965.
19. P. Aella, C. Cook, J. Tolle, S. Zollner, A. V. G. Chizmeshya, and J. Kouvetakis, "Optical and structural properties of  $\text{Si}_x\text{Sn}_y\text{Ge}_{1-x-y}$  alloys," *Appl. Phys. Lett.*, vol. 84, no. 6, p. 888, 2004.
20. a. Jamshidi, M. Noroozi, M. Moeen, a. Hallén, B. Hamawandi, J. Lu, L. Hultman, M. Östling, and H. Radamson, "Growth of GeSnSiC layers for photonic applications," *Surf. Coatings Technol.*, vol. 230, pp. 106–110, Sep. 2013.
21. Y. Nakamura, A. Masada, and M. Ichikawa, "Quantum-confinement effect in individual  $\text{Ge}_{1-x}\text{Sn}_x$  quantum dots on Si(111) substrates covered with ultrathin  $\text{SiO}_2$  films using scanning tunneling spectroscopy," *Appl. Phys. Lett.*, vol. 91, no. 1, p. 013109, 2007.
22. R. Chen, Y.-C. Huang, S. Gupta, A. C. Lin, E. Sanchez, Y. Kim, K. C. Saraswat, T. I. Kamins, and J. S. Harris, "Material characterization of high Sn-content, compressively-strained GeSn epitaxial films after rapid thermal processing," *J. Cryst. Growth*, vol. 365, pp. 29–34, Feb. 2013.
23. J. Kouvetakis and A. V. G. Chizmeshya, "New classes of Si-based photonic materials and device architectures via designer molecular routes," *J. Mater. Chem.*, vol. 17, no. 17, p. 1649, 2007.